Molecular Genetics and Metabolism xxx (xxxx) xxx

Contents lists available at ScienceDirect

Molecular Genetics and Metabolism

journal homepage: www.elsevier.com/locate/ymgme

Deficiency of the sedoheptulose kinase (Shpk) does not alter the ability of hematopoietic stem cells to rescue cystinosis in the mouse model

Spencer Goodman [a,1], Meisha Khan [a,1], Jay Sharma [a], Zijie Li [a], Jose Cano [a], Carlos Castellanos [a], Monica V. Estrada [b], Ilya Gertsman [c], Stephanie Cherqui [a,*]

[a] Department of Pediatrics, Division of Genetics, University of California, San Diego, La Jolla, CA, USA
[b] Tissue Technology Shared Resource, Biorepository and Tissue Technology, Moores Cancer Center, University of California, San Diego, La Jolla, CA, USA
[c] Clarus Analytical, LLC, San Diego, CA, USA

ARTICLE INFO

Article history:
Received 20 September 2021
Received in revised form 9 November 2021
Accepted 10 November 2021
Available online xxxx

Keywords:
Cystinosis
Sedopheptulose kinase
Pentose phosphate pathway
Hematopoietic stem and progenitor cells
Macrophages

ABSTRACT

Cystinosis is an autosomal recessive lysosomal storage disorder caused by mutations in the *CTNS* gene encoding the lysosomal cystine transporter, cystinosin, and leading to multi-organ degeneration including kidney failure. A clinical trial for cystinosis is ongoing to test the safety and efficacy of transplantation of autologous hematopoietic stem and progenitor cells (HSPCs) *ex vivo* gene-modified to introduce functional *CTNS* cDNA. Preclinical studies in $Ctns^{-/-}$ mice previously showed that a single HSPC transplantation led to significant tissue cystine decrease and long-term tissue preservation. The main mechanism of action involves the differentiation of the transplanted HSPCs into macrophages within tissues and transfer of cystinosin-bearing lysosomes to the diseased cells via tunneling nanotubes. However, a major concern was that the most common cystinosis-causing mutation in humans is a 57-kb deletion that eliminates not only *CTNS* but also the adjacent sedopheptulose kinase *SHPK*/*CARKL* gene encoding a metabolic enzyme that influences macrophage polarization. Here, we investigated if absence of *Shpk* could negatively impact the efficiency of transplanted HSPCs to differentiate into macrophages within tissues and then to prevent cystinosis rescue. We generated *Shpk* knockout mouse models and detected a phenotype consisting of perturbations in the pentose phosphate pathway (PPP), the metabolic shunt regulated by SHPK. $Shpk^{-/-}$ mice also recapitulated the urinary excretion of sedoheptulose and erythritol found in cystinosis patients homozygous for the 57-kb deletion. Transplantation of $Shpk^{-/-}$-HSPCs into $Ctns^{-/-}$ mice resulted in significant reduction in tissue cystine load and restoration of *Ctns* expression, as well as improved kidney architecture comparable to WT-HSPC recipients. Altogether, these data demonstrate that absence of SHPK does not alter the ability of HSPCs to rescue cystinosis, and then patients homozygous for the 57-kb deletion should benefit from *ex vivo* gene therapy and can be enrolled in the ongoing clinical trial. However, because of the limits inherent to animal models, outcomes of this patient population will be carefully compared to the other enrolled subjects.

1. Introduction

Cystinosis is an autosomal recessive lysosomal storage disorder caused by mutations in the *CTNS* gene that affects one out of every 100,000 to 200,000 live births [1]. *CTNS* encodes a proton-driven transmembrane lysosomal cystine transporter, cystinosin [2]. Over 100 unique mutations have been identified that perturb the localization or function of the cystinosin protein, ranging from single base substitutions to large indels [2–4]. Loss of the ubiquitously expressed cystinosin leads to lysosomal cystine accumulation and crystallization throughout the body, causing multisystemic organ failure [5]. Renal Fanconi syndrome presents in infants as the first clinical manifestation, and patients progressively develop end-stage renal failure, photophobia, myopathy, diabetes, hypothyroidism and neurological defects [1,6]. The main targeted therapeutic is the drug cysteamine, which facilitates lysosomal cystine export, prolonging life expectancy to early adulthood [7]. However, severe side-effects and extremely frequent and burdensome dosing lead to issues with patient compliance and, ultimately, this treatment merely delays symptomatic progression [8].

We pioneered a new treatment to address the root genetic cause of cystinosis by utilizing a hematopoietic stem and progenitor cell (HSPC) gene therapy approach [9]. Extensive preclinical experimentation using

* Corresponding author at: University of California, San Diego, Department of Pediatrics, Division of Genetics, 9500 Gilman Drive, MC 0734, La Jolla, CA, USA.
E-mail address: scherqui@ucsd.edu (S. Cherqui).
[1] Equal first authors.

https://doi.org/10.1016/j.ymgme.2021.11.006

the C*tns*$^{-/-}$ mouse model established that a single transplantation of wildtype (WT) HSPCs lead to lifelong morphological and functional preservation of affected tissues including the kidney, cornea and thyroid [10–13]. Mechanism of action studies revealed that therapeutic efficacy relies upon HSPC differentiation into macrophages within tissues and delivery of cystinosin-bearing lysosomes to the diseased cells via open-ended membranous protrusions known as tunneling nanotubes (TNTs) [14,15]. Promising results in mice led to the initiation of a phase 1/2 clinical trial in which cystinosis patients undergo autologous transplantation of HSPCs, modified *ex vivo* using a lentiviral vector to express functional *CTNS* (ClinicalTrials.gov Identifier #NCT03897361).

However, the mechanism of action underlying HSPC-mediated tissue preservation in cystinosis raised a concern for subject selection in the clinical trial. Indeed, the most common mutation in cystinosis is a large 57 k base pair (kb) deletion spanning not only the *CTNS* gene, but also the entirety of the adjacent sedoheptulokinase (*SHPK, a.k.a CARKL)* locus [16]. About 40% of human cystinosis patients are homozygous for the 57-kb deletion and so lack any functional copy of *SHPK,* a metabolic enzyme that regulates the formation of sedoheptulose-7-phosphate (S7P) which is a key component of the non-oxidative arm of the pentose phosphate pathway (PPP) [17]. Alterations of PPP products and intermediates have been detected in patients' urine and blood spots [18,19]. Importantly, SHPK was shown to regulate macrophage polarization and differentiation by altering the PPP flux [20]. As HSPC therapy relies on differentiation of functional macrophages, it is critical to determine if patients carrying the 57-kb deletion at the homozygous state would still benefit from the stem cell gene therapy approach.

To address this issue, we generated and characterized two novel *Shpk*-deficient mouse models (*Shpk*$^{-/-}$ mice). These mice exhibit alterations of PPP in liver and urine. We transplanted *Ctns*$^{-/-}$ mice with HSPCs isolated from *Shpk*$^{-/-}$ mice and demonstrated their ability of rescue cystinosis as assessed by reduction in tissue cystine accumulation, restoration of *Ctns* expression, and preservation of renal morphology. Our results indicate that cystinosis patients lacking SHPK are equally likely to receive therapeutic benefit from autologous transplantation of gene-modified HSPCs and will be enrolled in the clinical trial.

2. Material and methods

2.1. Mice and ethics statement

C57BL/6 J *Ctns*$^{-/-}$ mice were provided by Dr. Antignac (Inserm U983, Paris, France). Shpk$^{\Delta ATG}$ (C57BL/6 J *Shpk*$^{-/-}$) mice were generated at the UCSD Mouse Genomics Core using CRISPR/Cas9 and sgRNA targeting the start codon of Shpk genomic locus. Shpk$^{\Delta E2}$ (C57BL/6 *Shpk*$^{-/-}$) mice were generated at the Mutant Mouse Resource & Research Center at UC Davis using CRISPR/Cas9 and sgRNA targeting exon 2 of *Shpk*. Both strains were also crossbred with transgenic DsRed (B6.Cg-Tg(CAG-DsRed*MST)1Nagy/J) mice provided by the Jackson Laboratory (Bar Harbor, ME) to establish colored lines with constitutive expression of DsRed fluorescent protein (DsRed^{+}*Shpk*$^{-/-}$ mice). All strains and mouse procedures were approved by the University of California, San Diego (UCSD) in accordance with the guidelines set forth by the Institutional Animal Care and Use Committee (Protocol ID #S12288).

2.2. Mouse genotyping

Shpk mutant status was identified using PCR-based genotyping assays from mouse tail tissue. DirectPCR (Tail) (Viagen) and Protinease K treatment of mouse tails was used for DNA extraction. PCR protocol of Shpk$^{\Delta ATG}$ DNA amplification is as follows: 95 °C (3 min) initial denaturation; 30 cycles of 98 °C (20 s) denaturation, 65 °C (15 s) annealing, and 72 °C (15 s) extension; and 72 °C (1 min/kb) final extension. Resultant wild-type band sizes were 632 bp; and mutant size was 495 bp. PCR protocol of Shpk$^{\Delta E2}$ DNA amplification was provided by UC Davis and is as follows: 94 °C (2 min) initial denaturation; 10 cycles of 94 °C (10 s) denaturation, 65 °C (15 s) annealing with consecutive runs lowering in temperature by 1 °C (−1 °C/cycle), and 68 °C (2 min) extension; and 25 cycles of 94 °C (2 min) denaturation, 65 °C annealing (30 s), and 68 °C (2 min) extension with consecutive runs increasing in duration by 20 s (+20 s/cycle). Resultant wild-type band sizes were 638 and 1184 bp; and mutant size was 500 bp. Primer sequences can be found in Table S1.

2.3. Real time-qPCR

RNeasy Mini Kit and protocol (Qiagen, Hilden, Germany) was used for whole RNA extraction; blood RNA was extracted using the RNeasy Protect Animal Blood Kit (Qiagen). cDNA synthesis occurred by reverse transcription of 1 μg tissue and blood RNA using iScript cDNA Synthesis Kit (Bio-Rad, Hercules, CA). RT-qPCR reaction assembly consisted of 5 ul iTaq Universal SYBR Green, 3 μL cDNA (5 ng/ul), 0.6 μL forward and reverse primer (10 μM), and 1.8 μL H20, and ran on a CFX96 thermocycler (Bio-Rad) under the following conditions: 95 °C (30 s); 40 cycles of 95 °C (5 s) and 60 °C (30 s); then 65 °C (5 s); and 95 °C (5 s). Gene expression was measured using the delta/delta CT method relative to glyceraldehyde 3-phosphate dehydrogenase (*Gapdh*). All primer sequences are shown in Table S1.

2.4. Immunoblotting

RIPA lysis buffer (Sigma, St Louis, MO) composed of protease/phosphatase inhibitor cocktail (Thermo Fisher Scientific, Waltham, MA) was used for protein lysis. The Pierce BCA Protein Assay Kit (Thermo Fisher Scientific) was used to calibrate protein concentrations. SDS-NuPAGE treatment of 10–20 μg of protein were ran on 4–12% Bis-Tris Gel (Novex by Life Technologies, Carlsbad, CA) and transferred to PVDF membranes. Primary incubation with anti-Shpk antibody (Sigma; 1:2000) ran at 4 °C overnight. The next day, membranes were washed three times in Protein Wash Buffer (Azure Biosystems, Dublin, CA) and incubated in HRP-conjugated secondary antibodies goat anti-rabbit and rhodamine anti-tubulin (BioRad; 1:2000) for 1 h at RT. Membranes are again washed three times and a final time in 1× tris buffered saline (TBS). Blots were activated by HRP substrate Radiance Plus ECL Reagent (Azure) and chemiluminescent detection was captured on the c600 Imager (Azure). Western blots were quantitated by comparative densitometry against tubulin loading control.

2.5. Metabolomics

Harvested livers were rapidly freeze-clamped and placed in ice-cold liquid nitrogen to preserve robust metabolic activity. Samples were then powderized and 20 mg was resuspended in extraction solution (40% methanol/40% acetonitrile/20% H_20) supplemented with 40 μL ^{13C}-labeled internal standards (Cambridge Isotype Laboratories) per mL solution. Samples were homogenized using Precellys® homogenizer, immediately returned to dry ice for 1 h, then spun at 13000 xg for 15 mins. Supernatant was then lyophilized on a speed vac with cold trap to dryness, and then injected onto an LC-MS/MS system (API 4500 triple quadrupole MS, AB Sciex) for quantification of metabolites of interest (PPP intermediates, glycolytic intermediates, and nucleotides), as thoroughly described in the supplementary methods. Multiple batches from different collections were scaled together using WT controls, with a scale factor applied that preserved the intra-batch fold changes between the different cell types. This data is presented in the box plots in terms of relative abundance in relation to the controls. Urine analysis of erythritol, erythronic acid, and sedoheptulose was also performed using a separate LC-MS/MS method, as also described in the Supplementary Methods. Calibration curves, chromatograms, and QC performance for this method are found in Fig. S3.

2.6. HSPC isolation and transplantation

HSPC isolation and transplantation were performed as previously described [9]. In brief, bone marrow fluid was flushed from harvested tibias and femurs of donor wild-type, Ctns$^{-/-}$, Shpk$^{\Delta ATG}$, and Shpk$^{\Delta E2}$ mice. Sca1^{+} HSPCs were isolated by immunomagnetic separation using magnetic beads conjugated to anti-Sca1 antibody (Miltenyi Biotec, Auburn, CA). *Ctns*$^{-/-}$ mice were lethally irradiated (6.5 Gy; X-Rad 320, PXi) 24 h prior injection of 100 μL of PBS containing 1×10^6 HSPCs via tail vein. At ~6 months post-transplantation, recipient mice were sacrificed and kidney, liver, and spleen samples were isolated for analyses of therapeutic efficacy.

2.7. Cystine content

Tissue cystine was measured as previously described [9]. Briefly, explanted tissues were homogenized using the Precellys 24 homogenizer (Bertin Technologies) N-ethylmaleimide (Fluka Biochemika). Lysates were transferred to 15% % 5-sulfosalicylic acid (SSA) (Fluka Biochemika) and centrifuged to remove proteins for comparative quantitation using BCA assay (Pierce). The cystine-containing supernatants were transferred to 3% SSA and diluted before being quantitated by mass spectrometry at the UCSD Biochemical Genetics as described previously [21].

2.8. Histology

To assess general tissue morphology, dissected tissues were fixed in 10% formalin for 48 h and then transferred to the UCSD Moores Cancer Center Biorepository & Tissue Technology Center. Samples were embedded in paraffin, sectioned at 4 μm and stained with hematoxylin&Eosin (H&E) staining to assess histologic anomalies. For kidney, further analysis was done to quantify the extent of cortical damage as previously described [13]. To estimate the extend of the affected parenchyma in kidneys, periodic acidshift (PAS) staining was also performed, which stains basement membrane, so is useful for evaluating glomerular cell number, basement membrane, mesangium, tubular basement membrane and apical end of the proximal convoluted tubule epithelium's brush border [22]. All kidney's H&E and PAS slides were blindly scored by Dr. Valeria Estrada (Tissue Technology Shared Resource, Moores Cancer Center, UCSD) based on extent of cortical damage; a grade of 1 corresponded to 0–10% damage, Grade 2 to 10–30%, Grade 3 to 30–50% and Grade 4 to 50–70% [13].

2.9. Immunofluorescence

Tissues were fixed in 4% paraformaldehyde, dehydrated in 20% sucrose and mounted in Tissue Tek Optimum Cutting Temperature (OCT) stored at −80 °C. Tissues were cut into 16 μm-wide sections and placed on IHC slides. For staining, slides were washed in PBS three times for 10 min at RT, treated with blocking buffer (1% BSA, 5% goat serum, 0.3% triton X-100) for 1 h at RT, and probed with macrophage markers anti-F4/80 (Santa Cruz; 1:50) and anti-MHCII (BD Biosciences; 1:50) primary antibodies overnight at 4 °C. The following day, slides were washed in PBS three times and probed with secondary antibodies anti-rabbit AF562 and phalloidin AF647 for 1 h at RT. After two more 10-min PBS washes and a final PBS and DAPI (1:1000) wash, slides were mounted with glass slips using Prolong Gold. The following day, images were taken using the LSM 880 confocal microscope (Zeiss).

2.10. Renal function

24-h urine collections were preformed using metabolic cages with collection over ice and treated with 100× Protease Inhibitors. Serum was obtained from survival retro-orbital bleeding and placed in heparin tubes for blood chemistry including creatinine, albumin, urea, phosphorus and protein, and in EDTA tubes for complete blood count; both being measured at UCSD ACP Veterinary Diagnostic Laboratory Service. Urine creatinine, phosphate and glucose were measured using colorimetric assays according to the manufacturer recommendations (BioAssay Systems, Hayward, CA). Total proteinuria was measured using Pierce BCA Protein Assay Kit (Thermo Fisher Scientific).

2.11. Statistics

All statistics were analyzed using Graphpad Prism 9 software. Briefly, Student's *t*-test was used for comparisons of two groups, and one-way analysis of variance (ANOVA) for comparisons of three or more conditions with Tukey's multiple comparison test used to evaluate differences between individual groups. All graphs display mean ± standard error of the mean (sem).

3. Results

3.1. Shpk knockout generation and expression characterization

To obtain a source of *Shpk*-deficient HSPCs, we generated two novel *Shpk* knockout (*Shpk*$^{-/-}$) mouse models using CRISPR-Cas9 guides to create heritable homozygous indels via non-homologous end joining (Fig. 1A). We observed stable and heritable transmission of two *Shpk* genomic frameshift deletions; a 168-bp deletion centered around the start codon (*Shpk*$^{\Delta ATG}$), and a 675-bp elimination of the entire second exon (*Shpk* $^{\Delta E2}$) (Fig. S1 and Table 1 for primer sequences). Heterozygote

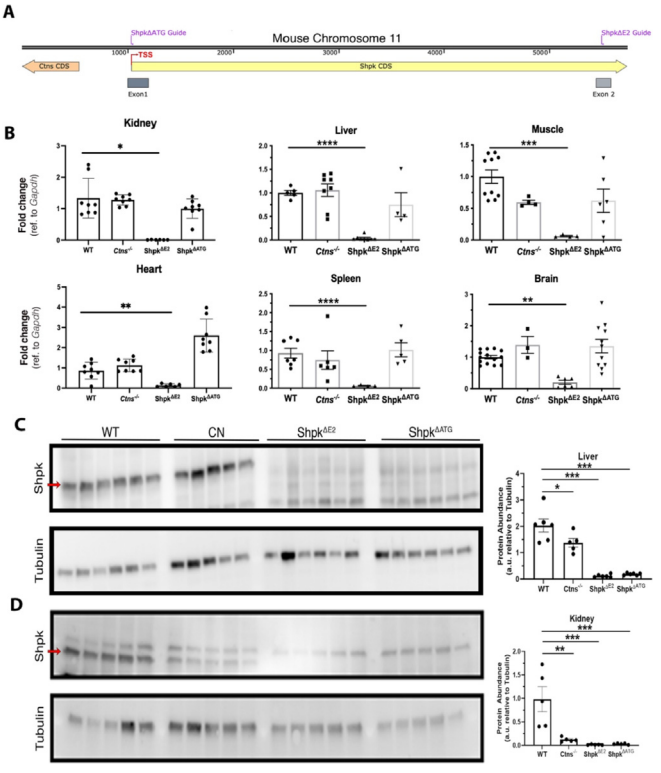

Fig. 1. Generation and characterization of two novel Shpk knockout mouse models. (**A**) Diagram of the mouse genomic region between *Ctns* and *Shpk*. CRISPR-Cas9 guides depicted at start codon (Shpk$^{\Delta ATG}$) or second exon (Shpk$^{\Delta E2}$). CDS: coding DNA sequence, TSS: transcription start site. (**B**) *Shpk* expression as measured by qPCR in various tissues from the Shpk-knockout mice as compared to WT and *Ctns*$^{-/-}$ mice. Data are mean ± standard deviation (SD) (**C**–**D**) Representative western blot showing SHPK expression in liver (**C**) and kidney (**D**) from WT, *Ctns*$^{-/-}$, *Shpk*$^{\Delta ATG}$, and *Shpk*$^{\Delta E2}$ mice with anti-tubulin as loading control. Quantitation is based on relative densitometry between size-appropriate SHPK band and tubulin. Data are mean ± sem. * $P < 0.05$, ** $P < 0.01$, *** $P < 0.001$ relative to WT.

Table 1
Renal function markers in the urine and serum.

	WT ($n = 3$)	Ctns$^{-/-}$ ($n = 5$)	Ctns$^{-/-}$ HSPC ($n = 8$)	WT HSPC ($n = 11$)	Shpk$^{-/-}$ HSPC ($n = 18$)	Reference Ranges*
Serum						
Creatinine (mg/dL)	0.2 ± 0.0	0.2 ± 0.0	0.2 ± 0.0	0.3 ± 0.0	0.2 ± 0.0	0.2–0.8
Blood Urea Nitrogen (mg/dL)	17.7 ± 3.7	23 ± 2.0	29.4 ± 1.9	31.7 ± 4.4	30.1 ± 3.4	18–29
Phosphorus (mg/dL)	5.9 ± 1.3	4.7 ± 0.5	5.7 ± 0.3	5.6 ± 0.3	6.6 ± 0.4	6.1–10.1
Albumin (g/dL)	3.7 ± 0.2	3.6 ± 0.1	3.5 ± 0.1	3.5 ± 0.1	3.6 ± 0.1	2.5–4.8
Total Protein (g/dL)	4.4 ± 0.3	4.4 ± 0.2	4.7 ± 0.2	4.6 ± 0.1	4.7 ± 0.1	3.6–6.6
	WT ($n = 4$)	Ctns$^{-/-}$ ($n = 7$)	Ctns$^{-/-}$ HSPC ($n = 12$)	WT HSPC ($n = 13$)	Shpk$^{-/-}$ HSPC ($n = 27$)	Reference Ranges*
Urine						
Polyuria (mL)	1.04 ± 0.19	3.31 ± 0.79[a]	1.20 ± 0.26[b]	1.41 ± 0.25[b]	1.70 ± 0.28[b]	
Phosphate/creatinine (μmol/μmol Cr)	25.53 ± 4.50	31.61 ± 4.51	31.30 ± 5.55	31.43 ± 3.63	39.35 ± 6.74	
Protein/creatinine (mg/mgCr)	0.60 ± 0.03	3.66 ± 1.89	6.35 ± 1.91	4.42 ± 1.86	3.97 ± 1.03	
Glucose/creatinine (mg/mgCr)	2.56 ± 0.93	17.48 ± 5.55	13.78 ± 3.34	6.26 ± 0.97	10.43 ± 3.62	

Data are presented as mean ± sem.
Urine data are from 24-h urine measures and reported to urine creatine ratio.
* Normal range for C57BL/6 mice – Charles River.
[a] $p < 0.05$ *vs.* WT mice.
[b] $p < 0.05$ *vs.* Ctns$^{-/-}$ mice.

mice were bred and *Shpk*$^{-/-}$ mice were obtained following a mendelian ratio in both models.

We then characterized *Shpk* mRNA and protein expression as a measure of knockout efficacy. Real-time quantitative-PCR (RT-qPCR) analysis confirmed a dramatic reduction of *Shpk* expression in *Shpk*$^{\Delta E2}$ tissues compared to WT controls (Fig. 1B). In contrast, *Shpk* mRNA expression in *Shpk*$^{\Delta ATG}$ tissues retained variable levels of transcription with no significant differences in any tissue compared to WT samples. However, by immunoblotting we detected a strong size-appropriate band of 57-kilodaltons (kD) in WT and *Ctns*$^{-/-}$ liver and kidney that were completely absent in both *Shpk*$^{\Delta E2}$ and *Shpk*$^{\Delta ATG}$ mice (Fig. 1C–D). These results indicate that despite residual mRNA expression in *Shpk*$^{\Delta ATG}$, neither knockout mouse model resulted in any translated SHPK protein. Surprisingly, significantly decreased SHPK expression was detected in the *Ctns*$^{-/-}$ liver and kidney compared to WT (Fig. 1D), the reason of these results is unknown. SHPK protein was not detected in WT brain, heart, spleen, and muscle (data not shown). Histological analysis of kidney and liver from *Shpk*$^{\Delta E2}$ and *Shpk*$^{\Delta ATG}$ mice did not reveal any obvious difference compared to WT mice (data not shown). Note that this model does not recapitulate the patients' 57 kb-deletion that remove both *CTNS* and *SHPK* genes. However, the because the gene therapy approach restores *CTNS* in patients' HSPCs, they also become only *SHPK*-deficient.

3.2. Pentose Phosphate Pathway (PPP) metabolomics are disrupted in *Shpk*$^{-/-}$ liver and urine

Phosphorylation of sedoheptulose into sedoheptulose-7-phosphate (S7P) via SHPK enzymatic activity is an important step in the pentose phosphate pathway (Fig. 2A) [23,24]. We assessed PPP metabolite abundance by intracellular mass spectrometry in flash-frozen liver samples to determine if genetic ablation of *Shpk* resulted in a metabolic phenotype. We specifically focused on the following PPP metabolites: i) S7P as the direct *Shpk* product; ii) glyceraldehyde-3-phosphate as an aldose intermediate (measured together with its isomer dihydroxacetone phosphate); iii) erythrose-4-phosphate (E4P), a downstream erythritol precursor; and iv) upstream intermediates ribose-5-phosphate (measured together with its isomer xyulose-5-phosphate), and 6-phosphogluconate (6PG) [20,25]. We observed an expected reduction in S7P abundance, indicating direct enzymatic loss-of-function in both *Shpk*$^{-/-}$ strains (Fig. 2B). We also observed reduction of all other analytes compared to WT and *Ctns*$^{-/-}$ (Fig. 2B). Furthermore, as altered

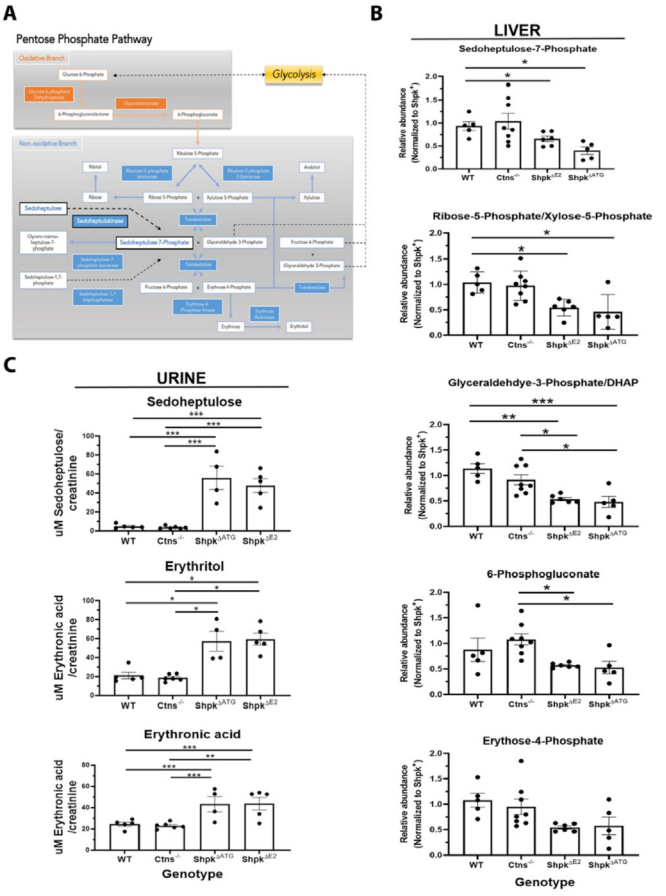

Fig. 2. Elimination of *Shpk* leads to metabolic perturbations in the pentose phosphate pathway. (**A**) Schematic of the pentose phosphate pathway (PPP) illustrating reactions, intermediates and SHPK metabolism of implicated metabolites. **(B)** Mass spectrometry quantitation of PPP metabolite relative abundance in WT, *Ctns*$^{-/-}$, *Shpk*$^{\Delta ATG}$, and *Shpk*$^{\Delta E2}$ livers ($n = 4$–6). **(C)** Mass spectrometry quantitation of urinary PPP metabolic content ($n = 4$–6). Statistical significance was determined using one-way ANOVA followed by Tukey's multiple comparison test. Data are mean ± sem * $P < 0.05$, ** $P < 0.01$, *** $P < 0.001$.

Shpk expression corresponded with imbalances in cellular redox states [20,25], we also examined in *Shpk*$^{-/-}$ liver the status of energy carriers (Fig. S2A), hexose sugars (Fig. S2B) or acetyl coA (Fig. S2C). With the exception of a decrease of hexose sugars (glucose and fructose) and AMP in *Shpk*$^{-/-}$ samples, no significant changes were detected between the different groups. These findings indicate that *in vivo* elimination of SHPK yields a phenotype of PPP dysregulation in liver without marked changes in overall cellular energy balance.

Clinical analysis of human cystinosis patients homozygous for the 57-kb deletion revealed urinary secretion of sedoheptulose and erythritol [19]. Thus, we examined PPP associated metabolites (sedoheptulose, erythronic acid, and erythritol) in urine from *Shpk*-deficient mice. We detected significant increases in urinary sedoheptulose and erythritol in *Shpk*$^{-/-}$ mice as compared to either WT and *Ctns*$^{-/-}$ mice (Fig. 2C). These results demonstrate the first *in vivo* models of PPP dysregulation. The new mouse models appear to successfully phenocopy understudied aspects of metabolic dysregulation in cystinosis, and further highlights on as-yet-unknown aspects of more global perturbation of the PPP in tissues deficient for SHPK.

3.3. *Shpk*$^{-/-}$ HSPC transplantation reduced cystine level and restored *Ctns* expression across multiple tissues of recipient cystinotic mice

Following generation and characterization of *Shpk*$^{-/-}$ mice, we evaluated the therapeutic efficacy of *Shpk*$^{-/-}$-HSPC transplantation for cystinosis disease prevention to predict if cystinosis patient homozygous for the 57-kb deletion would benefit from the stem cell gene therapy. Donor Sca1^{+} HSPCs were immunomagnetically harvested from the bone marrow of 6-8-week-old *Shpk*$^{\Delta ATG2}$ and *Shpk*$^{\Delta E2}$ mice and transplanted into 2-month-old lethally irradiated *Ctns*$^{-/-}$ mice. As positive, we also transplanted WT-HSPCs in *Ctns*$^{-/-}$ mice [9,12,13]. As negative controls, we used *Ctns*$^{-/-}$ mice untreated or transplanted with *Ctns*$^{-/-}$-HSPCs; no significant difference existing between these two groups for cystine and *Ctns* expression analysis (data not shown). As both *Shpk*$^{-/-}$ mouse models resulted from a complete knockout of SHPK expression and in similar metabolic phenotype (Figs. 1C, 2 and S2) and because there was no significant difference between these two groups for cystine and *Ctns* expression analysis (data not shown), recipients of *Shpk*$^{\Delta ATG2}$ and *Shpk*$^{\Delta E2}$ HSPCs were pooled for downstream analysis.

Proper bone marrow reconstitution and hematopoiesis was obtained in the *Ctns*$^{-/-}$ mice transplanted by *Ctns*$^{-/-}$, WT and *Shpk*$^{-/-}$-HSPCs as evidenced by complete blood counts (Table S2). Effectiveness of HSPC transplantation for cystinosis can best be assessed by quantifying cystine content across various body tissues. In liver, spleen, muscle, brain, and eye, cystine level was significantly reduced in both WT- and *Shpk*$^{-/-}$-HSPC-transplanted *Ctns*$^{-/-}$ mice compared to *Ctns*$^{-/-}$ controls (Fig. 3A). As sex-specific differences in cystine accumulation have been observed specifically in the kidney [9], kidney cystine content data were analyzed in males and females separately, cystine was reduced in both male and female *Shpk*$^{-/-}$-HSPC-transplanted *Ctns*$^{-/-}$ kidneys compared to controls but significant only in females (Fig. 3A). An additional indication of transplantation efficacy is *Ctns* mRNA expression, which is normally absent from *Ctns*$^{-/-}$ animals. *Ctns* mRNA expression was measured in the liver, spleen, brain, and kidney of *Ctns*$^{-/-}$ mice in the different groups. As compared to *Ctns*$^{-/-}$ controls, mice injected with *Shpk*$^{-/-}$-HSPCs had significantly higher *Ctns* expression across all tissues at a level comparable to WT-HSPC recipients (Fig. 3B). Altogether, these data demonstrate that *Shpk*$^{-/-}$-HSPCs are equally efficacious as WT-HSPCs at exogenous restoration of *Ctns* expression and subsequent reduction of cystine accumulation.

3.4. *Shpk*$^{-/-}$ HSPC transplantation improves kidney function and morphology in *Ctns*$^{-/-}$ mice

It was previously shown that WT-HSPCs were able to preserve kidney function and structure [13]. In the past, C57BL/6 *Ctns*$^{-/-}$

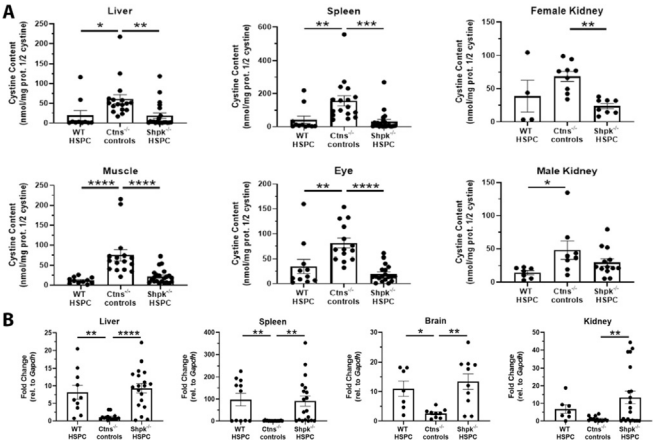

Fig. 3. Transplantation of *Shpk*-deficient HSPCs into cystinosis mice effectively reduced cystine accumulation and restored *Ctns* expression. (A) Tissue cystine content in *Ctns*$^{-/-}$ mice transplanted with WT- and *Shpk*$^{-/-}$-HSPCs compared to *Ctns*$^{-/-}$ controls. (B) *Ctns* mRNA expression across several tissues in *Ctns*$^{-/-}$ mice transplanted with WT- and *Shpk*$^{-/-}$-HSPCs compared to *Ctns*$^{-/-}$ controls. Data are mean ± sem. * $P < 0.05$, ** $P < 0.01$, *** $P < 0.001$ relative to *Ctns*$^{-/-}$ controls.

robustly demonstrated Fanconi syndrome markers such as glucosuria, phosphaturia, proteinuria and polyuria, and developed chronic kidney disease [26]. However, a steady decrease of symptomatic severity of kidney defects has been observed by multiple independent investigators using the same mouse model, potentially due to genetic drift. Thus, as expected, no major difference was observed between WT and *Ctns*$^{-/-}$ mice for kidney function (Table 1). Only polyuria was significantly increased in *Ctns*$^{-/-}$ mice compared to WT mice, and was significantly reduced in *Ctns*$^{-/-}$-, WT- and *Shpk*$^{-/-}$-HSPCs transplanted *Ctns*$^{-/-}$ mice (Table 1).

Renal architecture was evaluated by histological analysis scoring in blind with scores ranging from 1 to 6 based on the percent extent of cortical damage as previously described [13]. Irradiation causes tissue anomalies so untreated and *Ctns*$^{-/-}$-HSPC *Ctns*$^{-/-}$ recipients were evaluated separately. The severity of kidney damage was significantly lower in WT-HSPC and *Shpk*$^{-/-}$-HSPC *Ctns*$^{-/-}$ recipients as compared to *Ctns*$^{-/-}$-HSPCs *Ctns*$^{-/-}$ mice (Fig. 4). The main anomalies consisted in glomerulosclerosis, dilated or atrophic convoluted proximal tubules, thickening of the basement membranes, protein casts, and mononuclear infiltrates, which were seen predominantly in the *Ctns*$^{-/-}$-HSPC *Ctns*$^{-/-}$ mice (Fig. 4). Therefore, both WT-HSPCs and *Shpk*$^{-/-}$-HSPCs conferred a protective effect on kidney morphological structure in *Ctns*$^{-/-}$ mice.

3.5. Transplanted *Shpk*$^{-/-}$-HSPC progeny are capable of tissue integration and differentiation into macrophages

Delivery of functional cystinosin to diseased cells relies on tissue integration of HSPC-derived macrophages. To characterize HSPC-derived cells *in vivo*, we generated DsRed^{+}*Shpk*$^{-/-}$ mice and isolated HSPCs for visualization and characterization of their progeny within tissues after transplantation in *Ctns*$^{-/-}$ mice. As control, DsRed^{+}WT^{-}-HSPCs were transplanted in *Ctns*$^{-/-}$ mice. In liver and kidney, DsRed-positive cells co-colocalized with the macrophage markers F4/80 and MHCII in *Shpk*$^{-/-}$-HSPC recipient mice, identifying these cells as macrophages (Fig. 5) as previously shown for WT-HSPCs [9,11–13,15]. MHCII being a marker of M1-like macrophages, theses data suggest that *Shpk*$^{-/-}$-HPSCs differentiate into a typical pro-inflammatory macrophage phenotype as we previously described for cystinosis [15]. These data indicate that *Shpk*-deficiency does not impact HSPC-derived macrophage differentiation following transplantation in *Ctns*$^{-/-}$ mice.

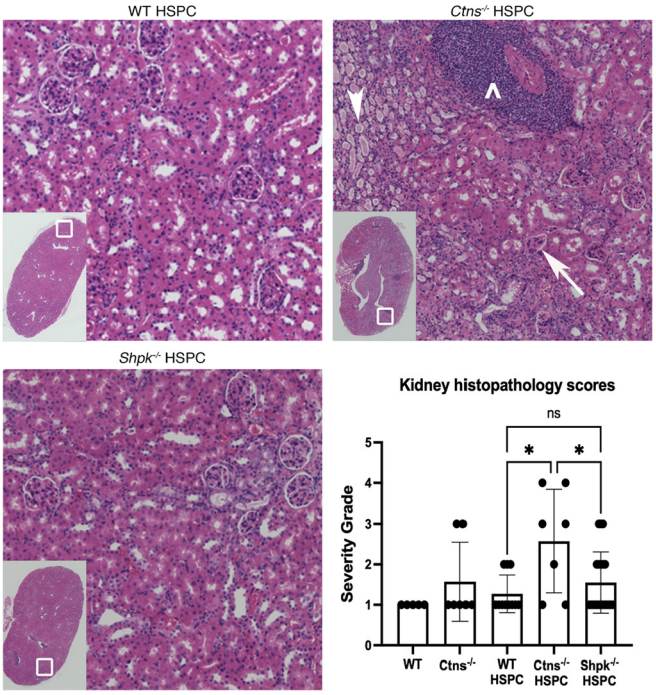

Fig. 4. Transplantation of *Shpk*-deficient HSPCs into Ctns$^{-/-}$ mice preserves kidney morphology. Representative kidney sections stained with hematoxylin & eosin of 8-month-old *Ctns*$^{-/-}$ mice that received either WT-HSPCs, *Shpk*$^{-/-}$-HSPCs or *Ctns*$^{-/-}$-HSPCs. Samples were graded in blind based on cortical damage – see Methods for details. Glomerulosclerosis (arrow), protein casts (arrowhead) and mononuclear infiltrates (^) could be observed especially in the *Ctns*$^{-/-}$-HSPC recipients. Statistical significance was determined using one-way ANOVA followed by Tukey's multiple comparison test. Data are mean ± sem * $P < 0.05$.

4. Discussion

The present study characterized the first murine models of Shpk knockout, and the potential impact of the absence of SHPK on the HSPC transplantation therapy for cystinosis. This question has direct relevance for the ongoing clinical trial for cystinosis as a large fraction of human cystinosis patients are homozygous for the 57-kb deletion leading to the lack of *SHPK* in addition to *CTNS* gene. Indeed, HSPC therapy is mediated by differentiation of HSPCs into macrophages [14], and SHPK has been shown to be involved in the regulation of macrophage polarization [20].

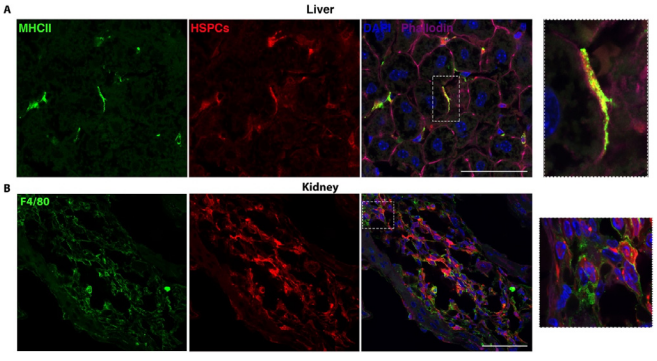

Fig. 5. *Shpk*-deficient HSPCs retain the ability to differentiate into macrophages after transplantation in liver and kidney. **(A** and **B)** Representative confocal images showing co-localization between transplanted DsRed^{+}*Shpk* $^{-/-}$-HSPCs (red) and the macrophage markers MHCII (**A**) or F4/80 (**B**) in recipient *Ctns*$^{-/-}$ livers (**A**) and kidney (**B**). F-actin visualized via phalloidin staining is shown in purple, and the nuclei stained with dapi is shown in blue. Scale bars, 100 μm. (For interpretation of the references to colour in this figure legend, the reader is referred to the web version of this article.)

To investigate if Shpk-deficient HSPCs were still able to rescue cystinosis, we first generated two new mouse models knockout for Shpk with deletions at two different loci of the murine *Shpk*; absence of SHPK protein was confirmed in both models. The mice did not present any obvious phenotype, breeding with mendelian ratio and exhibiting normal growth and behavior. SHPK/CARKL transcripts were previously detected mainly in liver, kidney, and pancreas, with weaker expression in heart, placenta, brain, and lung [16]. While *Shpk* mRNA expression was observed in kidney, liver, muscle, heart, spleen and brain in our WT and *Ctns*$^{-/-}$ mice, we only detected SHPK protein expression in the liver and kidney. No histological anomalies were found in kidney and liver of the two *Shpk*$^{-/-}$ mouse models. In contrast, perturbation of the Pentose Phosphate Pathway (PPP) was demonstrated in both mouse models. SHPK is part of the carbohydrate kinase family that phosphorylate sugars as they enter the cells to prevent their efflux [16]. SHPK enzyme is involved in the phosphorylation of sedoheptulose into sedoheptulose-7-phosphate (S7P) [19], which is part of the PPP, and, as expected, the *Shpk*$^{-/-}$ mice exhibited reduction of S7P.

It was unclear if absence of SHPK in cystinosis patients led to any pathologic phenotype. A small study reported no obvious clinical difference between patients carrying mutations causing infantile cystinosis and the ones carrying the 57-kb deletion [27]. However, more recently, two unrelated patients homozygous for nonsense mutation in *SHPK* were reported with strong but non-overlapping clinical phenotype so the attribution of SHPK was not conclusive [28]. Because no obvious phenotype or histological defects were found in the *Shpk*$^{-/-}$ mouse models, our results suggest that no major consequences should result from its deletion in patients carrying the 57-kb deletion at the homozygote state. One particularly interesting finding is that our mouse models effectively recapitulate urinary accumulation of the PPP metabolites erythritol and sedoheptulose seen in the patients affected with cystinosis [19]. While sedoheptulose accumulation made sense to the authors, they questioned the relevance of elevated erythritol with *SHPK* deficiency [19]. Our findings demonstrated that only *Shpk,* but not *Ctns,* knockout mice demonstrated elevated urinary sedoheptulose and erythritol providing further independent evidence that the loss of *SHPK* itself contributes to this phenotype in cystinosis [28]. However, the mechanism leading to increase erythritol secretion was unclear. A potential explanation was reported as sedoheptulose accumulation results in its conversion to S1P by fructokinase that would be converted to erythrose and then reduced to erythritol [23]. In addition, we showed that PPP metabolite perturbation was also present in the liver of *Shpk*$^{-/-}$ mice, suggesting that this pathway is also dysregulated in tissues in cystinosis patients in addition to urine and bloodspots.

The plasticity of macrophage polarization allows them to fulfill numerous biological functions ranging from pro-inflammatory roles classified as either pro-inflammatory mediator of a type I immune response (M1 macrophages), to tissue repair, homeostasis and resolution of inflammation (M2 macrophages) [29,30]. In the context of our stem cell trial for cystinosis, an important function of SHPK was reported by Haschemi and colleagues on its involvement in macrophage polarization [20]. Following lipopolysaccharide (LPS)-induced pro-inflammatory stimulation, *SHPK*-overexpressing in murine cultured macrophages showed decreased bio-abundance of PPP intermediates G3P, and R5P/X5P while unstimulated *SHPK*-knockdown macrophages showed conversely increased levels, as well as reduced S7P levels [20]. *SHPK*-knockdown promoted differentiation of the macrophages towards an M1-like phenotype. We showed previously that *in vitro* M1-like macrophages have decreased ability to generate tunneling nanotubes involved in lysosomal cross-correction in the hematopoietic stem cell-mediated therapy in cystinosis as opposed to M2-like macrophages [15]. However, *in vivo* we observed that transplantation of HSPCs isolated from *Rac2*$^{-/-}$ mice in which M2-like differentiation is disrupted still resulted in therapeutic efficacy in *Ctns*$^{-/-}$ mice,

suggesting complex influence of the environmental milieu in macrophage differentiation. In the present study, in contrast to the results obtained in cultured macrophages [20], our *Shpk*$^{-/-}$ mouse models yielded a general reduction in bio-abundance of R5P as well as both upstream and downstream PPP intermediates 6PG, E4P, and S7P in the liver without external LPS stimulation. 6PG and E4P were not measured in the previous study [20], so it is not clear to what extent the PPP is different between these two studies, but as *Shpk* has been implicated with regulating glucose metabolism and regulating metabolic state [20, 28, 31], it is not surprising that *Shpk*$^{-/-}$ may result in a more global perturbation of the PPP pathway beyond affecting S7P, though the mechanism is still undefined.

In the limit of the current *Ctns*$^{-/-}$ mouse model that presents a milder phenotype than human, this study allowed us through a variety of metrics including HSPC tissue integration and differentiation, kidney histology, tissue *Ctns* expression, and tissue cystine levels, to confirm that *Ctns*$^{-/-}$ recipients of *Shpk*$^{-/-}$-HSPCs showed significant improvements of diseased conditions. Altogether, these data strongly suggest that macrophage differentiation towards a pro- or anti- inflammatory response is dictated by the environmental milieu that may overcome genetic perturbation of their polarization. Given the well-known difficulty of macrophage polarization in culture to translate to the more complex *in vivo* environment, our data highlights the importance of *in vivo* exploration of *in vitro* findings to better represent physiological complexity.

In conclusion, this study reports the first characterization of the *Shpk*$^{-/-}$ mice recapitulating the urinary excretion of sedoheptulose and erythritol found in cystinosis patients homozygous for the 57-kb deletion, and suggesting that the PPP metabolic perturbation is also present in their tissues but with minimal consequences in tissue function and architecture. Our results also highlight the importance of *in vivo* models in the study of macrophage polarization that may respond to complex cell milieu that cannot be reproduced *in vitro*. As such, we showed that *Shpk*-deficient HSPCs will likely offer therapeutic efficacy in cystinosis patients carrying the 57-kb deletion at the homozygote state so these patients can now be enrolled in the ongoing stem cell gene therapy clinical trial for cystinosis, while careful comparison of the outcomes of this patient population will be performed with the rest of the enrolled subjects.

Author contributions statement

SG and MK conceived the experiments, analyzed the data, and wrote the manuscript. JS, ZL, and JC conducted the experiments. VE reviewed in blind the histological tissue sections and scored the kidney anomalies. IG performed the metabolomics studies. S.C conceived and supervised the study and wrote the manuscript. All authors reviewed the manuscript.

Declaration of Competing Interest

Stephanie Cherqui is co-inventor on a patent entitled “Methods of treating lysosomal disorders” (#20378–101,530), and is a cofounder, shareholder and a member of both the Scientific Board and board of directors of Papillon Therapeutics Inc. Stephanie Cherqui serves as a consultant for AVROBIO and receives compensation for these services. Stephanie Cherqui also serves as a member of the Scientific Review Board and Board of Trustees of the Cystinosis Research Foundation. The terms of this arrangement have been reviewed and approved by the University of California San Diego in accordance with its conflict of interest policies.

Acknowledgments

The authors thank Dr. Corinne Antignac for providing *Ctns*$^{-/-}$ mice as well as the UCSD Mouse Genomics Core and the Mutant Mouse Resource & Research Center at UC Davis for the generation of the Shpk knockout mouse models. The authors thank Anaëlle Ghezail and Jonathan Moreil, Riley Stack, and other lab members for their contributions. This work was supported by the Cystinosis Research Foundation, the National Institute of Health (NIH) RO1-DK090058 and R01-NS108965, the California Institute of Regenerative Medicine (CIRM, CLIN2-11478). UCSD Neuroscience Microscopy Shared Facility was funded by the Grant P30-NS047101.

Appendix A. Supplementary data

Supplementary data to this article can be found online at https://doi.org/10.1016/j.ymgme.2021.11.006.

References

[1] F. Emma, G. Nesterova, C. Langman, A. Labbe, S. Cherqui, P. Goodyer, M.C. Janssen, M. Greco, R. Topaloglu, E. Elenberg, R. Dohil, D. Trauner, C. Antignac, P. Cochat, F. Kaskel, A. Servais, E. Wuhl, P. Niaudet, W. Van't Hoff, W. Gahl, E. Levtchenko, Nephropathic cystinosis: an international consensus document, Nephrol. Dial. Transplant 29 (Suppl 4) (2014) iv87-94.

[2] V. Kalatzis, S. Cherqui, C. Antignac, B. Gasnier, Cystinosin, the protein defective in cystinosis, is a H(+)-driven lysosomal cystine transporter, EMBO J. 20 (2001) 5940–5949.

[3] S. Cherqui, C. Sevin, G. Hamard, V. Kalatzis, M. Sich, M.O. Pequignot, K. Gogat, M. Abitbol, M. Broyer, M.C. Gubler, C. Antignac, Intralysosomal cystine accumulation in mice lacking cystinosin, the protein defective in cystinosis, Mol. Cell. Biol. 22 (2002) 7622–7632.

[4] D. David, S. Princiero Berlingerio, M.A. Elmonem, F. Oliveira Arcolino, N. Soliman, B. van den Heuvel, R. Gijsbers, E. Levtchenko, Molecular basis of cystinosis: geographic distribution, functional consequences of mutations in the CTNS gene, and potential for repair, Nephron 141 (2019) 133–146.

[5] C. Chiaverini, H.Y. Kang, L. Sillard, E. Berard, P. Niaudet, G. Guest, M. Cailliez, P. Bahadoran, J.P. Lacour, R. Ballotti, J.P. Ortonne, In vivo reflectance confocal microscopy of the skin: a noninvasive means of assessing body cystine accumulation in infantile cystinosis, J. Am. Acad. Dermatol. 68 (2013) e111–e116.

[6] S. Baumner, L.T. Weber, Nephropathic Cystinosis: symptoms, treatment, and perspectives of a systemic disease, Front Pediatr 6 (2018) 58.

[7] A. Brodin-Sartorius, M.J. Tete, P. Niaudet, C. Antignac, G. Guest, C. Ottolenghi, M. Charbit, D. Moyse, C. Legendre, P. Lesavre, P. Cochat, A. Servais, Cysteamine therapy delays the progression of nephropathic cystinosis in late adolescents and adults, Kidney Int. 81 (2012) 179–189.

[8] S. Cherqui, Cysteamine therapy: a treatment for cystinosis, not a cure, Kidney Int. 81 (2012) 127–129.

[9] F. Harrison, B.A. Yeagy, C.J. Rocca, D.B. Kohn, D.R. Salomon, S. Cherqui, Hematopoietic stem cell gene therapy for the multisystemic lysosomal storage disorder cystinosis, Mol. Ther. 21 (2013) 433–444.

[10] H.P. Gaide Chevronnay, V. Janssens, P. Van Der Smissen, C.J. Rocca, X.H. Liao, S. Refetoff, C.E. Pierreux, S. Cherqui, P.J. Courtoy, Hematopoietic stem cells transplantation can normalize thyroid function in a cystinosis mouse model, Endocrinology 157 (2016) 1363–1371.

[11] C.J. Rocca, A. Kreymerman, S.N. Ur, K.E. Frizzi, S. Naphade, A. Lau, T. Tran, N.A. Calcutt, J.L. Goldberg, S. Cherqui, Treatment of inherited eye defects by systemic hematopoietic stem cell transplantation, Invest. Ophthalmol. Visual Sci. 56 (2015) 7214–7223.

[12] K. Syres, F. Harrison, M. Tadlock, J.V. Jester, J. Simpson, S. Roy, D.R. Salomon, S. Cherqui, Successful treatment of the murine model of cystinosis using bone marrow cell transplantation, Blood 114 (2009) 2542–2552.

[13] B.A. Yeagy, F. Harrison, M.C. Gubler, J.A. Koziol, D.R. Salomon, S. Cherqui, Kidney preservation by bone marrow cell transplantation in hereditary nephropathy, Kidney Int. 79 (2011) 1198–1206.

[14] S. Naphade, J. Sharma, H.P. Gaide Chevronnay, M.A. Shook, B.A. Yeagy, C.J. Rocca, S.N. Ur, A.J. Lau, P.J. Courtoy, S. Cherqui, Brief reports: lysosomal cross-correction by hematopoietic stem cell-derived macrophages via tunneling nanotubes, Stem Cells 33 (2015) 301–309.

[15] S. Goodman, S. Naphade, M. Khan, J. Sharma, S. Cherqui, Macrophage polarization impacts tunneling nanotube formation and intercellular organelle trafficking, Sci Rep 9 (2019) 14529.

[16] J.W. Touchman, Y. Anikster, N.L. Dietrich, V.V. Maduro, G. McDowell, V. Shotelersuk, G.G. Bouffard, S.M. Beckstrom-Sternberg, W.A. Gahl, E.D. Green, The genomic region encompassing the nephropathic cystinosis gene (CTNS): complete sequencing of a 200-kb segment and discovery of a novel gene within the common cystinosis-causing deletion, Genome Res. 10 (2000) 165–173.

[17] C. Nagy, A. Haschemi, Sedoheptulose kinase regulates cellular carbohydrate metabolism by sedoheptulose 7-phosphate supply, Biochem. Soc. Trans. 41 (2013) 674–680.

[18] M.M. Wamelink, E.A. Struys, E.E. Jansen, H.J. Blom, T. Vilboux, W.A. Gahl, M. Komhoff, C. Jakobs, E.N. Levtchenko, Elevated concentrations of sedoheptulose in bloodspots of patients with cystinosis caused by the 57-kb deletion: implications for diagnostics and neonatal screening, Mol. Genet. Metab. 102 (2011) 339–342.

[19] M.M. Wamelink, E.A. Struys, E.E. Jansen, E.N. Levtchenko, F.S. Zijlstra, U. Engelke, H.J. Blom, C. Jakobs, R.A. Wevers, Sedoheptulokinase deficiency due to a 57-kb deletion in cystinosis patients causes urinary accumulation of sedoheptulose: elucidation of the CARKL gene, Hum. Mutat. 29 (2008) 532–536.
[20] A. Haschemi, P. Kosma, L. Gille, C.R. Evans, C.F. Burant, P. Starkl, B. Knapp, R. Haas, J.A. Schmid, C. Jandl, S. Amir, G. Lubec, J. Park, H. Esterbauer, M. Bilban, L. Brizuela, J.A. Pospisilik, L.E. Otterbein, O. Wagner, The sedoheptulose kinase CARKL directs macrophage polarization through control of glucose metabolism, Cell Metab. 15 (2012) 813–826.
[21] I. Gertsman, W.S. Johnson, C. Nishikawa, J.A. Gangoiti, B. Holmes, B.A. Barshop, Diagnosis and monitoring of cystinosis using immunomagnetically purified granulocytes, Clin. Chem. 62 (2016) 766–772.
[22] S.K. Agarwal, S. Sethi, A.K. Dinda, Basics of kidney biopsy: a nephrologist's perspective, Indian J. Nephrol 23 (2013) 243–252.
[23] T. Kardon, V. Stroobant, M. Veiga-da-Cunha, E.V. Schaftingen, Characterization of mammalian sedoheptulokinase and mechanism of formation of erythritol in sedoheptulokinase deficiency, FEBS Lett. 582 (2008) 3330–3334.
[24] M.M. Wamelink, E.A. Struys, C. Jakobs, The biochemistry, metabolism and inherited defects of the pentose phosphate pathway: a review, J. Inherit. Metab. Dis. 31 (2008) 703–717.
[25] A. Stincone, A. Prigione, T. Cramer, M.M. Wamelink, K. Campbell, E. Cheung, V. Olin-Sandoval, N.M. Gruning, A. Kruger, M. Tauqeer Alam, M.A. Keller, M. Breitenbach, K.M. Brindle, J.D. Rabinowitz, M. Ralser, The return of metabolism: biochemistry and physiology of the pentose phosphate pathway, Biol. Rev. Camb. Philos. Soc. 90 (2015) 927–963.
[26] N. Nevo, M. Chol, A. Bailleux, V. Kalatzis, L. Morisset, O. Devuyst, M.C. Gubler, C. Antignac, Renal phenotype of the cystinosis mouse model is dependent upon genetic background, Nephrol. Dial. Transplant. 25 (2010) 1059–1066.
[27] H.P. Gaide Chevronnay, V. Janssens, P. Van Der Smissen, F. N'Kuli, N. Nevo, Y. Guiot, E. Levtchenko, E. Marbaix, C.E. Pierreux, S. Cherqui, C. Antignac, P.J. Courtoy, Time course of pathogenic and adaptation mechanisms in cystinotic mouse kidneys, J. Am. Soc. Nephrol 25 (2014) 1256–1269.
[28] S.G. Heil, E. Levtchenko, L.A. Monnens, F.J. Trijbels, N.M. Van der Put, H.J. Blom, The molecular basis of dutch infantile nephropathic cystinosis, Nephron 89 (2001) 50–55.
[29] M.M. Wamelink, R.J. Ramos, A.P. van den Elzen, G.J. Ruijter, R. Bonte, L. Diogo, P. Garcia, N. Neves, B. Nota, A. Haschemi, I. Tavares de Almeida, G.S. Salomons, First two unrelated cases of isolated sedoheptulokinase deficiency: a benign disorder? J. Inherit. Metab. Dis. 38 (2015) 889–894.
[30] I. Tabas, K.E. Bornfeldt, Intracellular and intercellular aspects of macrophage immunometabolism in atherosclerosis, Circ. Res. 126 (2020) 1209–1227.